Pairwise Mobility of Metal−Metal Bonds in $(MeC_5H_4)_4Ru_4S_3(SMe)^{n+}$

Eric J. Houser, Anne Venturelli, Thomas B. Rauchfuss,* and Scott R. Wilson

School of Chemical Sciences, University of Illinois, Urbana, Illinois 61801

Received March 22, 1995[⊗]

This report describes studies on the mobility of metal−metal bonds within the frameworks of unsymmetrical Ru_4S_4 clusters. A low-symmetry derivative of $(MeC_5H_4)_4Ru_4S_4$ (**1**) was prepared by methylation with MeO_3SCF_3 (MeOTf) to give $[(MeC_5H_4)_4Ru_4S_3(SMe)]^+$ (**1**Me$^+$). Crystallographic characterization of [**1**Me]OTf revealed a distorted tetrahedron of Ru atoms with two Ru−Ru bonds and four Ru−Ru nonbonding contacts. The M−M and M−S distances demonstrate that the cluster geometry is little affected by methylation, as shown by the similarity of the cores in **1** and **1**Me$^+$. For example the Ru−S(Me) distances are only ca. 0.05 Å shorter than other comparable Ru−S contacts in the cluster. ^{1}H NMR studies indicate that the crystallographically determined structure is retained in solution; i.e., there are three types of (MeC_5H_4)Ru sites in a 1:2:1 ratio. At higher temperatures, line broadening of two of the $CH_3C_5H_4$ signals is observed, indicative of chemical exchange between (MeC_5H_4)Ru sites. Magnetization transfer experiments confirm chemical exchange between the major and one of the two minor (MeC_5H_4)Ru sites. This process requires the movement of *both* Ru−Ru bonds. Cyclic voltammetry shows that **1**Me$^+$ undergoes a 2 e oxidation at 480 mV vs **1**$^{2+/0}$. Studies using differential pulse voltammetry indicate that the $\Delta E_{1/2}$ separating the **1**Me$^{2+/0}$ redox events is ~10 mV. Oxidation of **1**Me$^+$ with 2 equiv of $(C_5H_5)_2FePF_6$ gave green-colored salts of **1**Me^{3+}. The high-temperature ^{1}H NMR spectra of **1**Me^{3+} indicate a 3:1 ratio of Ru sites consistent with time-averaged C_{3v} symmetry while the low-temperature spectrum indicates that the (MeC_5H_4)-Ru sites are nonequivalent.

Introduction

We recently described examples of metal clusters wherein metal−metal bonds migrate among the edges of tri- and tetrametallic frameworks, via the interchange of bonding and nonbonding metal−metal contacts.[1,2] The dynamics examined in our studies are intrinsically simple, since *only* the M−M bonds are affected. These rearrangements may be considered a form of valence isomerism as seen in bullvalene,[3] P_7^{3-},[4] and other main group clusters.[5] There are, of course, many situations where M−M bond migration is coupled to other processes such as ligand addition/dissociation, ligand migration, or electron transfer.[6] In such cases it is not possible to identify the relative energetic importance of scission/formation of M−M bonds vs other changes in the cluster.

An interesting example of M−M bond/no bond dynamics was found with $(MeC_5H_4)_4Ru_4S_4^{2+}$, a 66 e cluster featuring three Ru−Ru bonds of ca. 2.8 Å, as well as three Ru···Ru nonbonding contacts of >3.5 Å.[7,8] Low-temperature ^{1}H NMR spectra for this cation are consistent with an idealized C_2 symmetry, as confirmed in the solid state by X-ray crystallography, with two types of MeC_5H_4 sites. At higher temperatures the ^{1}H NMR spectrum simplifies such that the four MeC_5H_4 groups appear equivalent. This pattern was also observed for $(Me_3SiC_5H_4)_4Ru_4S_4^{2+}$ as well as $(MeC_5H_4)_4Ru_4Se_4^{2+}$.[7] In more recent work we have discovered mobile metal−metal bonds in the 70 e cluster $(C_5Me_5)_4Ir_4S_4^{2+}$ and the 50 e trinuclear cluster $(C_5Me_5)_3Ir_3S_2$.[1] The dynamics of $(C_5Me_5)_4Ir_4S_4^{2+}$ are particularly striking because they are associated with the migration of only one Ir−Ir bond (eq 1).

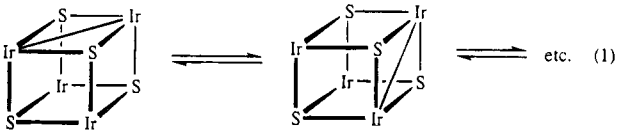

Ir = (C_5Me_5)Ir

In this study we return to the $(RC_5H_4)_4Ru_4S_4$ system in order to learn more about the nature of dynamics. We have synthesized a pair of derivatives of this cluster that allows us to probe two issues:

Effect of Mixed Valency on Metal−Metal Bond Mobility. The relocation of Ru−Ru bonds in $(RC_5H_4)_4Ru_4S_4^{2+}$ involves a formal intramolecular electron transfer process, as it interchanges Ru^{IV} and Ru^{III} sites.[7] Similarly, the dynamics of the Ir_4 and Ir_3 clusters involve formal interchange of Ir^{IV} and Ir^{III} or I^{III} and Ir^{II} sites, respectively. The question naturally arises as to whether mixed valency is a requirement for metal−metal bond mobility. Studies on homovalence clusters are therefore of interest. This issue could be probed using the 68 e parent $(MeC_5H_4)_4Ru_4S_4$,[9] wherein the four metals have the same oxidation state and the cluster features two Ru−Ru bonds. Unfortunately the dynamics in this cluster cannot be readily

[⊗] Abstract published in *Advance ACS Abstracts,* November 1, 1995.

(1) Venturelli, A.; Rauchfuss, T. B. *J. Am. Chem. Soc.* **1994**, *116*, 4824.
(2) Feng, Q.; Rauchfuss, T. B.; Wilson, S. R. *J. Am. Chem. Soc.* **1995**, *117*, 4702.
(3) (a) Doering, W. von E.; Roth, W. R. *Angew. Chem.* **1963**, *75*, 27. (b) Schröder, G. *Angew. Chem.* **1963**, *75*, 722.
(4) von Schnering, H. G. *Angew. Chem.* **1981**, *93*, 44; *Angew. Chem., Int. Ed. Engl.* **1981**, *20*, 33.
(5) von Schnering, H. G. In *Rings, Clusters, and Polymers of the Main Group Elements*; Cowley, A. H., Ed.; ACS Symposium Series 232; American Chemical Society: Washington, DC, 1983; pp 69−80.
(6) For examples see: (a) Edidin, R. T.; Zyzyck, L. A.; Norton, J. R. *J. Chem. Soc., Chem. Commun.* **1979**, 580. (b) Kubas, G. J.; Vergamini, P. J. *Inorg. Chem.* **1981**, *20*, 2667. (c) Bailey, D. A.; Balch, A. L.; Fossett, L. A.; Olmstead, M. M.; Reedy, P. E., Jr. *Inorg. Chem.* **1987**, *26*, 2413.
(7) Houser, E. J.; Rauchfuss, T. B.; Wilson, S. R. *Inorg. Chem.* **1993**, *32*, 4069. Houser, E. J.; Amaresekera, J.; Rauchfuss, T. B.; Wilson, S. R. *J. Am. Chem. Soc.* **1991**, *113*, 7440.
(8) A review of organometallic cubane clusters: Harris, S. *Polyhedron* **1989**, *8*, 2843.
(9) Amarasekera, J.; Rauchfuss, T. B.; Wilson, S. R. *J. Chem. Soc., Chem. Commun.* **1989**, 14.

0020-1669/95/1334-6402$09.00/0

assessed by NMR due to its highly symmetric structure. We have however found that it is possible to methylate one sulfur atom in $(MeC_5H_4)_4Ru_4S_4$, thereby lowering the cluster symmetry without introducing mixed valency.

Mobility of Metal−Metal Bond Pairs. Low-symmetry clusters might shed light on the pathways by which metal−metal bonds move within a cluster framework. For example, studies on $(C_5Me_5)_4Ir_4S_4^{2+}$ prove that the dynamics can proceed via the movement of one M−M bond.[1] Studies on the stereodynamics of $(RC_5H_4)_4Ru_4S_3(SMe)^+$ have allowed us to establish a dynamic pathway involving the coupled motion of two metal−metal bonds.

Results and Discussion

S-Methylation of $(MeC_5H_4)_4Ru_4S_4$. Dichloromethane solutions of $(MeC_5H_4)_4Ru_4S_4$ (**1**) react with 1 equiv of MeOTf to give $[(MeC_5H_4)_4Ru_4S_3(SMe)]^+$ (**1**Me$^+$) (eq 2) in 87% yield. The

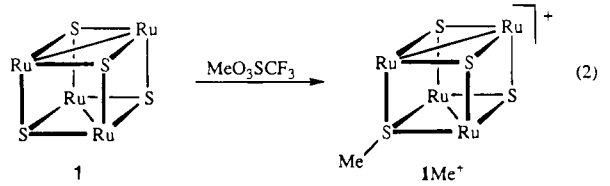

(2)

triflate salt of **1**Me$^+$ dissolves well in polar organic solvents to give red-brown moderately air stable solutions. Its IR spectrum is dominated by a band at 1266 cm^{-1} for ν_{SO} of the anion. The FAB mass spectrum shows the molecular ion, daughter peak envelopes corresponding to the demethylated cluster, and a series of fragments for $(MeC_5H_4)_{4-x}Ru_4S_4^+$. The ^1H and ^{13}C NMR spectra, which are interpreted in detail below, indicate that the $(MeC_5H_4)_4Ru_4S_4$ core remains intact insofar as the two Ru−Ru bonds remain nonadjacent.

NMR Spectra of $(MeC_5H_4)_4Ru_4S_3(SMe)^+$. The 500 MHz ^1H NMR spectrum of **1**Me$^+$ shows three singlets with a 2:1:1 intensity pattern in the 1.5−2.0 ppm region associated with three nonequivalent MeC_5H_4 groups. This pattern is consistent with methylation of **1** without changing the relative orientation of its Ru−Ru bonds. A singlet with a relative intensity of 3 observed at 2.72 ppm is assigned to the SCH_3. Seven distinct multiplets for MeC_5H_4 with relative intensities 1:2:1:1:1:1:1 were observed in the 6.0−4.0 ppm region (Figure 1). A total of eight multiplets are expected for MeC_5H_4, two of which are coincident, as indicated by the integrated intensities. The fact that ^3J(H,H) is small relative to the chemical shift range for MeC_5H_4 results in a spectrum that appears nearly first order.[10] The multiplets in the 4.0−6.0 ppm region also indicate three types of MeC_5H_4 groups, two of which are bisected by a mirror plane and a pair of which lie on either side of the same plane. The pair of equivalent MeC_5H_4 rings give rise to four multiplets (ABCD) while the two inequivalent MeC_5H_4 rings each appear as two multiplets (AA′BB′). The 2D NMR (COSY, 500 MHz) spectrum reveals three networks of MeC_5H_4 resonances (Figure 1). The four signals at 3.99, 4.59, 4.77, and 5.65 ppm are assigned to the symmetry equivalent MeC_5H_4 rings, and the resonances at 4.32 and 4.63 ppm each belong to one of the two chemically inequivalent MeC_5H_4 rings which share a coincident signal at 4.94 ppm. Using the COSY data, the MeC_5H_4 signals can be further assigned to α and β positions relative to the Me groups (details in the Experimental Section).

(10) Becker, E. D. *High Resolution NMR Theory and Chemical Applications*; Academic Press: New York, 1980; pp 88−93.

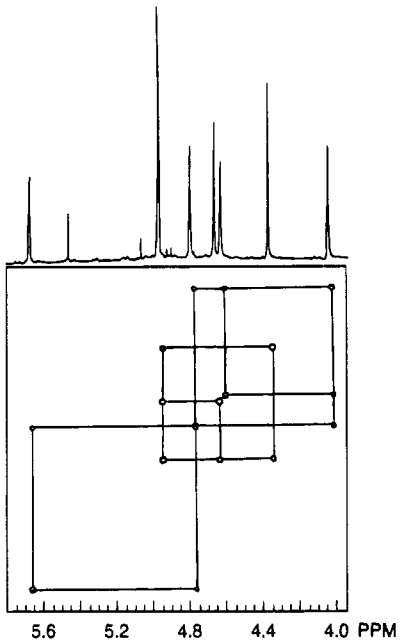

Figure 1. Two-dimensional 500 MHz (COSY) ^1H NMR spectrum of $[(MeC_5H_4)_4Ru_4S_3(SMe)]OTf$ (CD_3CN soln) in the MeC_5H_4 region.

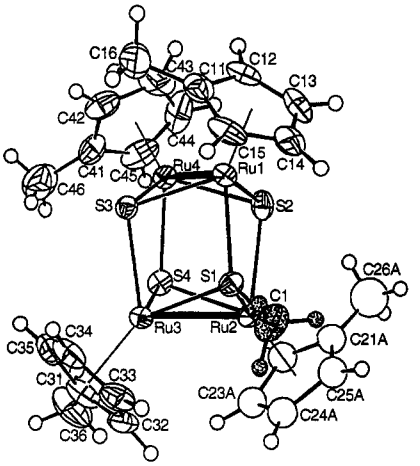

Figure 2. Structure of the cation $[(MeC_5H_4)_4Ru_4S_3(SMe)]^+$ with thermal ellipsoids drawn at the 30% probability level. The SCH_3 group is stippled.

The 125 MHz $^{13}C\{^1H\}$ NMR spectrum of a CD_3CN solution of **1**Me$^+$ shows three closely spaced singlets near 12.9 ppm in a 2:1:1 cation, assigned to $CH_3C_5H_4$ methyl groups, and another singlet at 35.2 ppm for μ_3-SCH_3. Eight signals in the 82−87 ppm region were assigned to the methyne centers, and the three closely spaced signals in the 105−106 ppm region are assigned to the *C*Me subunits. These data are consistent with the Ru_4S_3(SMe) core structure which was established by X-ray crystallography.

Solid State Structure of $[(MeC_5H_4)_4Ru_4S_3(SMe)](OTf)$. The structure of this salt was determined by single-crystal X-ray diffraction (Figure 2). The two bonding Ru−Ru distances are 2.788(1) and 2.789(1) Å while the four nonbonding Ru···Ru contacts range from 3.595(1) to 3.641(1) Å. For comparison the average bonding and nonbonding Ru−Ru distances in **1** are 2.76 and 3.60 Å, respectively.[7]

The structure of **1**Me$^+$ can be viewed as a nested pair of $(MeC_5H_4)_2Ru_2S_2$ and $(MeC_5H_4)_2Ru_2S(SMe)^+$ subunits, with each subunit containing a mutually bonded pair of Ru atoms. The S-methylation leads to contraction of the Ru−S distances by 2−3%. Within the $(MeC_5H_4)_2Ru_2S(SMe)^+$ subunit the Ru−

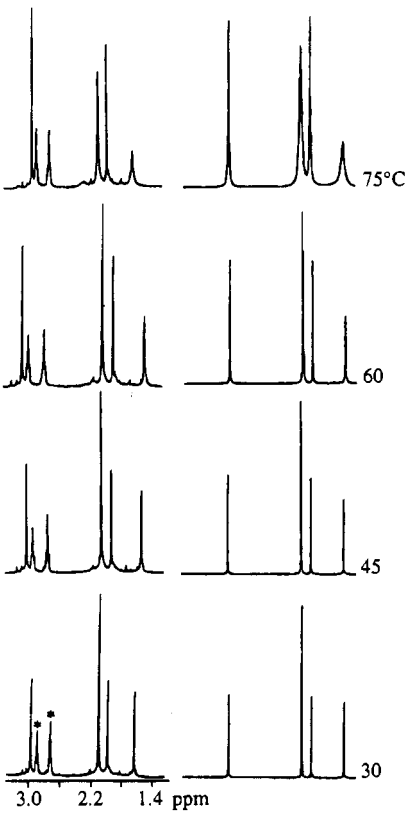

Figure 3. Variable-temperature 200 MHz ^{1}H NMR spectra of a DMF-d_7 solution of $[(MeC_5H_4)_4Ru_4S_3(SMe)]OTf$. The asterisks mark solvent peaks.

S(Me) distances are 2.264(3) and 2.269(3) Å while the other two Ru−S distances are 2.306(3) and 2.313(3) Å. The Ru−S distances between the Ru_2S_2 subunits range from 2.307(3) to 2.408(3) Å. Intersubunit S···S distances are 2.951(4) and 2.967(4) Å between μ_3-S, and 2.884(4) and 2.892(4) Å between μ_3-S and SMe sulfur atoms. The S···S contacts are 3.490(4) and 3.328(4) Å within the $(MeC_5H_4)_2Ru_2S_2$ and $(MeC_5H_4)_2Ru_2S(SMe)^+$ subunits, respectively. The $(MeC_5H_4)_2Ru_2S_2$ subunit features Ru−S−Ru angles of 73.20(9) and 73.78(8)° and S−Ru−S angles of 96.0(1) and 97.9(1)°. Similarly, within the $(MeC_5H_4)_2Ru_2S(SMe)^+$ subunit, the Ru−S−Ru angles are 74.25(9) and 75.91(9)° for the Ru−S−Ru and Ru−SMe−Ru angles, respectively, and the S−Ru−S angles are 93.29(10) and 93.3(1)°. The trends in the angle data are consistent with the greater steric bulk of the SMe group vs a sulfido atom.

Variable-Temperature NMR Studies on $(MeC_5H_4)_4Ru_4S_3(SMe)^+$. While the room-temperature ^{1}H NMR spectrum of $\mathbf{1Me}^+$ is consistent with the solid state structure, at higher temperatures (DMF-d_7 solution) two of the $CH_3C_5H_4$ resonances broaden (Figure 3). The unchanged $(CH_3C_5H_4)Ru$ signal is assigned to the position across the body center from the SMe group. Although coalescence was achieved at 105 °C, the higher temperature spectra were of poor quality.[11]

The dynamics of $\mathbf{1Me}^+$ were also examined by magnetization transfer methods. The advantage to this technique is that it is sensitive to the chemical exchange operating at a slower time scale than can be easily probed by classical coalescence behavior.[12] The limitations to the technique are twofold. First,

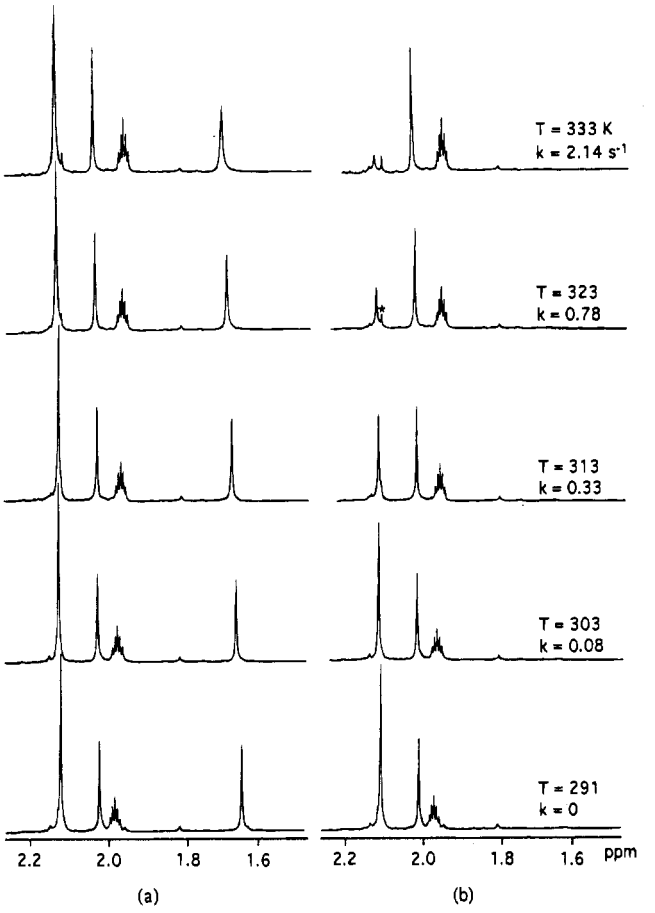

Figure 4. Magnetization transfer 400 MHz ^{1}H NMR spectra of an CD_3CN solution of $[(MeC_5H_4)_4Ru_4S_3(SMe)]OTf$ at various temperatures (a) before and (b) after irradiation. Only the data for the $CH_3C_5H_4$ region are shown. The asterisk marks a water peak.

chemical exchange must occur faster than the relaxation time of the nucleus probed. In this case the relevant relaxation times (30 °C) were approximately 3.5 s, corresponding to $k = 0.08$ s^{-1}. The second limitation to this technique is that it is incapable of distinguishing the effects of chemical exchange and nuclear Overhauser effects (nOe). The nOe problem is significant when the protons are held rigidly in close proximity; however, rotation about the MeC_5H_4 centroid is rapid. Furthermore, the crystallographic details of $\mathbf{1Me}^+$ allow us to gauge the range of H···H distances between the $CH_3C_5H_4$ centers. Molecular modeling methods confirm that while the methyl groups can in fact come into close contact, they typically would be >4 Å apart. The nonrigidity combined with the long H···H contacts would lead to minimal nOe effects.

In this experiment we saturated the more intense $CH_3C_5H_4$ signal and, after a delay, observed those sites to which this saturation transferred. This experiment was conducted at four temperatures over the range 18−60 °C (Figure 4). There is clearly exchange between the majority site and only one of the two minority sites. The exchange occurs between the same sites that were implicated in the above NMR line-broadening experiments. The temperature dependence of the exchange rates was evaluated by Eyring plots. In this way, we calculated values of $\Delta H^* = 88 \pm 10$ kJ/mol and $\Delta S^* = 25 \pm 31$ J/(mol K) (Table 2).

Oxidation of $[(MeC_5H_4)_4Ru_4S_3(SMe)]^+$. The redox properties of $\mathbf{1Me}^+$, as probed by cyclic voltammetry, consist of events centered at +260, −1150, and −1330 mV vs Ag/AgCl (Figure 5). Repeated cycles revealed the gradual demethylation of $\mathbf{1Me}^+$ to give **1**. The processes at negative potentials corre-

(11) The dynamics in $\mathbf{1Me}^+$ were modeled by computer simulation of the line shapes of the NMR spectra at four different temperatures, but the data are so far from the coalescence temperature that the calculated activation parameters may not be reliable: see ref 14.

(12) Freeman, R. *Handbook of Nuclear Magnetic Resonance*; John Wiley: New York, 1987; pp 198−202.

Table 1. Selected Distances (Å) and Angles (deg) in $[(MeC_5H_4)_4Ru_4S_3(SMe)]OTf$ ($\mathbf{1Me^+}$)

Ru1−Ru4	2.789(1)	Ru2−Ru3	2.788(1)
Ru1−Ru2	3.621(1)	Ru1−Ru3	3.630(1)
Ru2−Ru4	3.626(1)	Ru3−Ru4	3.595(1)
Ru1−S1	2.307(3)	Ru2−S1	2.264(3)
Ru1−S2	2.356(3)	Ru2−S2	2.408(3)
Ru1−S3	2.339(3)	Ru2−S4	2.313(3)
Ru3−S1	2.269(3)	Ru4−S2	2.321(3)
Ru3−S3	2.393(3)	Ru4−S3	2.306(3)
Ru3−S4	2.306(3)	Ru4−S4	2.361(3)
S1−C1	1.82(1)		
S1−Ru1−S2	76.7(1)	S1−Ru2−S2	76.4(1)
S1−Ru1−S3	76.75(10)	S1−Ru2−S4	93.29(10)
S2−Ru1−S3	96.0(1)	S2−Ru2−S4	77.3(1)
S1−Ru3−S3	76.37(10)	S2−Ru4−S3	97.9(1)
S1−Ru3−S4	93.3(1)	S2−Ru4−S4	78.1(1)
S3−Ru3−S4	78.3(1)	S3−Ru4−S4	78.91(9)
Ru1−S1−Ru2	105.6(1)	Ru2−S1−Ru3	75.91(9)
Ru1−S1−Ru3	105.0(1)	Ru2−S2−Ru4	100.1(1)
Ru1−S2−Ru2	99.7(1)	Ru2−S4−Ru3	74.25(9)
Ru1−S2−Ru4	73.20(9)	Ru2−S4−Ru4	101.7(1)
Ru1−S3−Ru3	100.2(1)	Ru3−S3−Ru4	99.8(1)
Ru1−S3−Ru4	73.78(8)	Ru3−S4−Ru4	100.8(1)

Table 2. Activation Parameters for M−M Bond Mobility in M_4S_4 Clusters[a]

cluster	$\Delta H^{\ddagger}$ (kJ/mol)	$\Delta S^{\ddagger}$ (J/(mol K))	solvent	ref
$[(MeC_5H_4)_4Ru_4S_4]^{2+}$	38 ± 2	−27 ± 9	CD_3CN	7
$[(C_5Me_5)_4Ir_4S_4]^{2+}$	80 ± 17	82 ± 29	CD_2Cl_2	1
$[(MeC_5H_4)_4Ru_4S_3(SMe)]^+$	88 ± 10	25 ± 31	CD_3CN	this work

[a] The parameters for the nonmethylated clusters were recalculated from previous data, assuming the error limits of ±2 K in temperature and 10% for rate constants.

sponds to reductions. The 260 mV event is a 2 e process, as indicated by the magnitude of the peak potentials (i_p), assigned to the $\mathbf{1Me^+}/\mathbf{1Me^{3+}}$ couple. This was confirmed by the preparative scale oxidation of $\mathbf{1Me^+}$ using 2 equiv of $(C_5H_5)_2FePF_6$ (eq 3).

$$(MeC_5H_4)_4Ru_4S_3(SMe)^+ \xrightarrow{2Fe(C_5H_5)_2^+} (MeC_5H_4)_4Ru_4S_3(SMe)^{3+} \quad (3)$$

The separation of the potentials for the two oxidations of $\mathbf{1Me^+}$ was examined by differential pulse voltammetry (DPV). This analysis relied on Richardson and Taube's relationship[13] between the width of the DPV peak and $\Delta E_{1/2}$. Our results indicate that $\Delta E_{1/2} \sim 10$ mV.

The $MeNO_2$-soluble $[(MeC_5H_4)_4Ru_4S_3(SMe)](OTf)(PF_6)_2$ was further characterized by mass spectrometry, micronalysis, and IR spectroscopy. Salts of $\mathbf{1Me^{3+}}$ are green (λ = 642 nm) whereas $\mathbf{1^{0/2+}}$ and $\mathbf{1Me^+}$ are red-brown. The fast atom bombardment (FAB) mass spectrum of the trication proved similar to that of the monocationic parent compound. The ^1H NMR resonance for SCH_3 shifts by 0.4 ppm downfield upon oxidation. Although the core of $\mathbf{1Me^{3+}}$ is demonstrably dynamic, we only observe one SCH_3 peak over the entire temperature range; thus, only one diastereoisomer is stable. Other details of the NMR data are discussed below.

Variable-Temperature NMR Studies on the Mixed Valence Cluster $(MeC_5H_4)_4Ru_4S_3(SMe)^{3+}$. The low-temperature (−25 °C) limiting ^1H NMR spectrum of $\mathbf{1Me^{3+}}$ features four $CH_3C_5H_4$ resonance consistent with a structure containing three

(13) Richardson, D. E.; Taube, H. *Inorg. Chem.* **1981**, *20*, 1278.

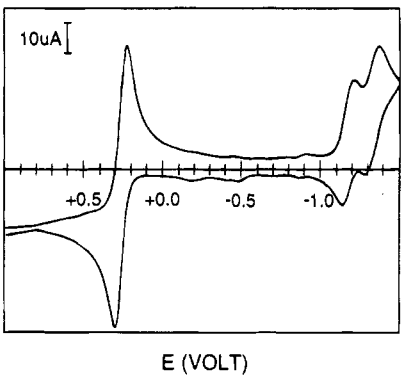

Figure 5. Cyclic voltammogram of 10^{-3} M solution of $[(MeC_5H_4)_4Ru_4S_3(SMe)]OTf$ in 0.1 M Bu_4NPF_6MeCN at a sweep rate of 100 mV/s (vs Ag/AgCl).

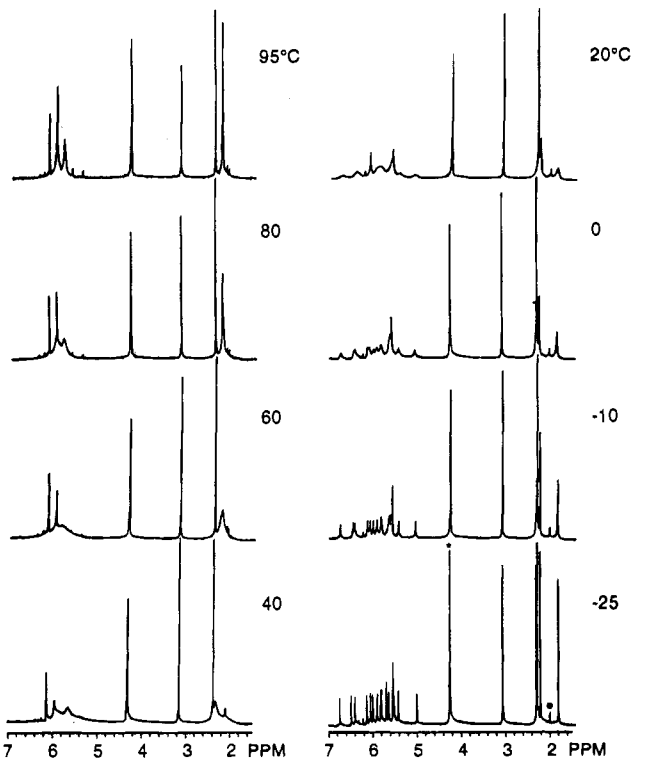

Figure 6. Variable-temperature 500 MHz ^1H NMR spectra of $[(MeC_5H_4)_4Ru_4S_3(SMe)](PF_6)_2OTf$ (CD_3NO_2 soln). The labeled peaks in the −25 °C spectrum are due to H_2O and CD_2HNO_2.

adjacent Ru−Ru bonds. All $CH_3C_5H_4$ sites are expected to be nonequivalent, and we were able to resolve fourteen of the expected sixteen signals (Figures 6 and 7). The fourteen resonances in the 5−7 ppm range can be further assigned by long-range COSY experiments, which identify four MeC_5H_4 coupling networks. The chemical shifts for two of these MeC_5H_4 networks are dispersed over ca. 1.5 ppm, and the other two have chemical shifts over a relatively narrow range of 0.5 ppm. Detailed assignments are presented in the Experimental Section, where it can be seen that eight of the signals are assignable to sites α to the methyl groups. The overall pattern is consistent with two pairs of similar MeC_5H_4 groups. These pairs of sites differ according to the number of Ru−Ru bonds (one or two). The NMR data show that $\mathbf{1^{2+}}$ exists predominantly as one diastereoisomer. S-Methylation of $\mathbf{1^{2+}}$ could produce two diastereoisomers, depending on which of the two types of sulfido atoms are attacked in this C_2 symmetric dication ($\mathbf{1Me^{3+}}$ was not prepared by methylation of $\mathbf{1^{2+}}$, but this is an easy way to visualize two of the possible isomers of $\mathbf{1Me^{3+}}$).

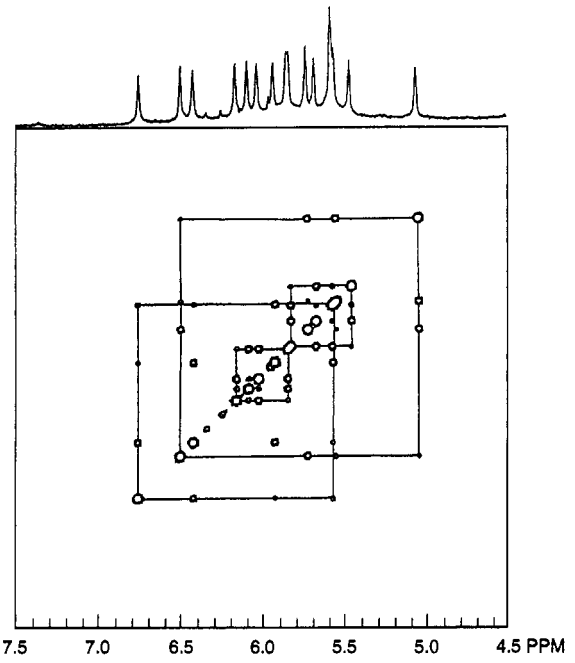

Figure 7. ^{1}H NMR COSY spectrum (500 MHz) of $[(MeC_5H_4)_4Ru_4S_3(SMe)](PF_6)_2OTf$ (CD_3NO_2 soln. −25 °C).

Higher symmetry arrangements of the three Ru−Ru bonds are not consistent with the NMR data (eq 4).

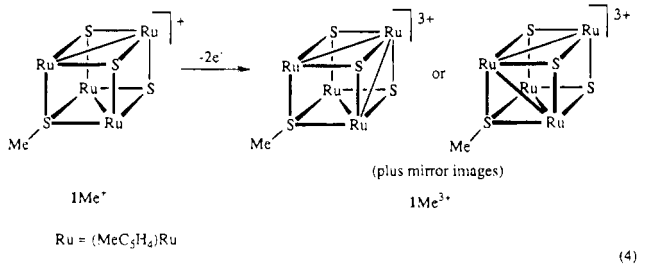

(4)

At 95 °C, the $CH_3C_5H_4$ resonances appear as a 3:1 ratio of $CH_3C_5H_4$ signals, consistent with the introduction of C_{3v} symmetry. At this temperature we were also able to resolve three of the expected four MeC_5H_4 signals. This observation that the dynamic process leads to racemization, as shown by the presence of only four (two overlapping) MeC_5H_4 resonances, which have a 1:4 (=1+3):3 intensity ratio in the high-temperature spectrum. If chirality were preserved in the dynamic process, then we would expect to see greater complexity, such as two ABCD patterns in a 3:1 ratio.

Turning to the $^{13}C\{^1H\}$ NMR data, the low-temperature (−25 °C) spectrum of a CD_3NO_2 solution of $\mathbf{1Me}^{3+}$ showed sixteen signals in the 89−97 ppm region assigned to methyne carbon centers (Figure 8). Four resonances were identified in the 116−124 ppm region for *C*Me centers. Additionally four resonances in the 13−15 ppm region were assigned to the $CH_3C_5H_4$ carbons and a signal at 36.65 ppm was assigned to μ_3-S*C*H$_3$. Overall the ^{13}C NMR results are completely consistent with the structures discussed above. Weak ^{13}C resonances assigned to the OTf^- anion were observed as a quartet centered at 117 ppm (J_{CF} = 74 Hz).

Pathways for Metal−Metal Bond Mobility in $\mathbf{1Me}^{3+}$. In this section we discuss the possible pathways for site exchange

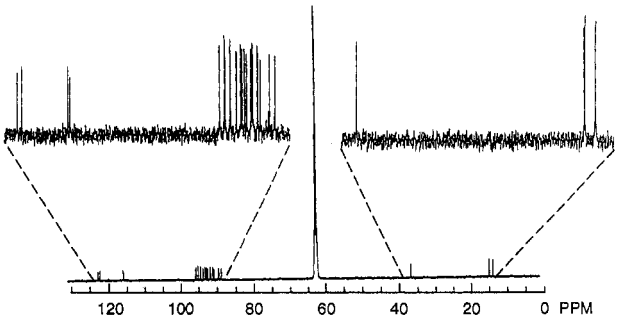

Figure 8. $^{13}C\{^1H\}$ NMR spectrum (125 MHz) of $[(MeC_5H_4)_4Ru_4S_3(SMe)](PF_6)_2OTf$ (CD_3NO_2 soln, −25 °C).

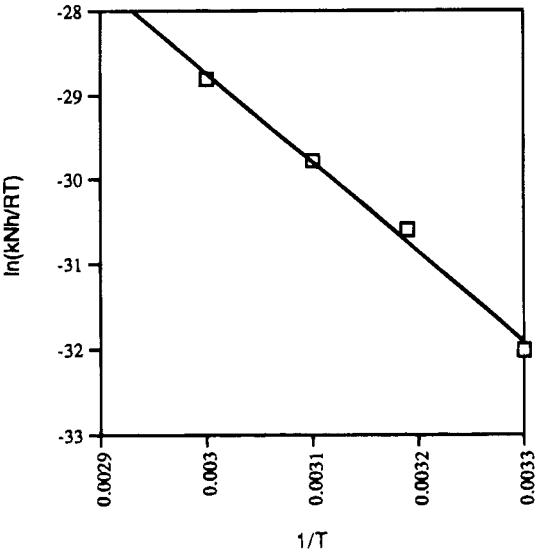

Figure 9. Plot of $\ln(kNh/RT)$ vs T^{-1}, where the k values were obtained by the magnetization transfer experiments on $\mathbf{1Me}^+$.

in the tricationic cluster.[14] We assume that the unique Ru atom (the one that is *not* bonded to μ_3-SMe) retains the same number of Ru−Ru bonds before and after the exchange process. This is justified by the relative constancy of the chemical shift and line width of the nonexchanging $CH_3C_5H_4$ signal. With this single constraint, as many as four exchange pathways can be identified (Scheme 1):[15] (i) interchange of a pair of Ru atoms (pairwise exchange) via migration of one of the terminal Ru−Ru bonds (Note that only one of two such bonds can migrate in a degenerate process.); (ii) pairwise exchange via migration of a central Ru−Ru bond; (iii) pairwise exchange via migration of both terminal bonds; and (iv) lastly, site exchange via a delocalized transition state of virtual C_{3v} symmetry.

The first pathway effectively introduces a plane of symmetry into the molecule. If this pathway were solely operative, we should observe signals for three types of MeC_5H_4 ligands at high temperatures. A similar argument applies to the second pathway. In *combination* these two processes can equilibrate three of the Ru sites, as required by the DNMR results. In the turnstile mechanism, the two terminal Ru−Ru bonds move, resulting in time-averaged C_s symmetry. This process is similar to that identified in $\mathbf{1Me}^+$. Summarizing, the fluxionality of $\mathbf{1Me}^{3+}$ can be explained by either (i) the simultaneous action

(14) For three-site exchange, there are $3!/h$ permutational isomerizations (h = order of molecular point group symmetry; in this case h = 1). Those permutational isomerizations include the identity operation (not an exchange process), three pairwise exchanges (see Scheme 1), and two cyclic permutations (arising from a C_3 intermediate).

(15) Houser, E. J. Ph.D. Thesis. University of Illinois at Urbana-Champaign, 1994.

Scheme 1

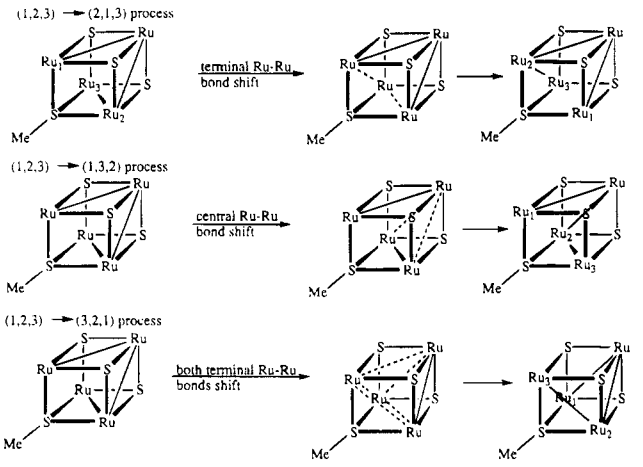

of at least two localized pathways (Scheme 1) or (ii) a fully delocalized intermediate of C_{3v} symmetry.

Conclusions

Synthesis and General Properties. S-Methylation of **1** is an efficient synthetic transformation that allows selective modification of the cluster. Preliminary experiments show that multiple methylation can occur with excess MeOTf.[16] A recent report by van den Berg et al. discusses the methylation of the *per*sulfide ligands in $(C_5H_5)_4Fe_4S_6$ and $(C_5H_5)_4Fe_4S_5$.[17]

The S-methylated cluster $\mathbf{1Me}^+$ has proven nearly ideal for studying the dynamics of metal−metal bonds. The symmetry of the cluster is lowered, but S-methylation does not prevent Ru−Ru bond movement in the mixed valence derivatives. Furthermore, the structural details of the Ru_4S_4 core are only slightly affected by the methylation. Compound **1** also represents a useful structural model for cluster protonation relevant to the ability of **1** to reduce protons to H_2.[15]

Redox Studies. The redox potentials for the couples $\mathbf{1Me}^+/\mathbf{1Me}^{2+}$ and $\mathbf{1Me}^{2+}/\mathbf{1Me}^{3+}$ are very similar. We had previously observed that the couples for $\mathbf{1}^{0/+}$ and $\mathbf{1}^{+/2+}$ are also close.[7] For comparison, the $E_{1/2}$ values relating the four oxidation states of $(C_5H_5)_4Fe_4S_4$ are separated by 0.66, 0.56, and 0.52 V.[18] The corresponding redox couples in $(C_5Me_5)_3(Ph_2C_2S_2)Fe_4S_3(S_2)$ are separated by 0.76, 0.44, and 0.61 V.[19] The $\Delta E_{1/2}$ values in these Fe_4 clusters can be attributed to the effect of on-site Coulombic repulsion associated with the change in the charge of the cluster.[20] The range of $\Delta E_{1/2}$ for these Fe_4 clusters of 0.4−0.6 V is comparable to the 0.48 V difference between the oxidation potentials of **1** and $\mathbf{1Me}^+$.

When a compound undergoes two redox events near the same potential, it is logical to assume that this reflects the ability of the cluster to disperse the charge introduced with the first redox event. This explanation might apply to the fact that $Fe_3(PR)_2(CO)_9$ (R = $M(CO)_2C_5H_5$; M = Mn, Fe) is reduced by 2 e at nearly a single potential.[21] In this case the thirteen CO ligands very effectively disperse the negative charge associated with the successive reductions. In contrast $\Delta E_{1/2}$ for $Fe_3(PPh)_2(CO)_9$ is 500 mV.[22] Even more extreme is the case of the related 50 e $(MeC_5H_4)_3Co_3S_2$ where $\Delta E_{1/2}$ = 780 mV.[23]

The absence of acceptor ligands in $(MeC_5H_4)_4Ru_4S_4$ and $(MeC_5H_4)_4Ru_4S_3(SMe)^+$ indicates that some factor other than charge dispersal is responsible for the small $\Delta E_{1/2}$. We propose that in the Ru_4S_4 clusters the destabilizing Coulomb potential is compensated by Ru−Ru bond formation. This requires that the enthalpic reward for making the Ru−Ru bond is primarily associated with the second oxidation step. Further insights come from a comparison of the oxidation potentials for the monocations $\mathbf{1}^+$ and $\mathbf{1Me}^+$. The $\mathbf{1}^{+/2+}$ couple is stabilized by 0.48 V with respect to the $\mathbf{1Me}^{+/2+}$ couple, reflecting the stabilizing influence provided by the formation of a new Ru−Ru bond. This supports our hypothesis that Ru−Ru bond formation occurs in the second oxidation step, i.e. in the conversion of $Ru^{III}_3Ru^{IV}$ to $Ru^{III}_2Ru^{IV}_2$. The fact that $[E_{1/2}(\mathbf{1}^{+/2+}) - E_{1/2}(\mathbf{1Me}^{+/2+})]$ is comparable to the $\Delta E_{1/2}$ values for $(C_5H_5)_4Fe_4S_4$ suggests that M−M bonding is energetically less important in Fe−S clusters.

Metal−Metal Bond Dynamics. The pair of Ru−Ru bonds in the homovalence cluster $\mathbf{1Me}^+$ are mobile. This was established by two types of DNMR experiments. The exchange process makes equivalent three of the four $(CH_3C_5H_4)Ru$ centers, consistent with the introduction of an effective C_3 symmetry axis. Since $\mathbf{1Me}^+$ is fluxional, it is very likely that **1** itself is also. It is interesting that the dynamics in $\mathbf{1Me}^+$ are subject to a higher barrier than those in $\mathbf{1}^{2+}$. This suggests that the energy barrier is related to the number of Ru−Ru bonds moved. Similar conclusions were reached by Kubas and Vergamini in their studies[6b] on $(C_5H_5)_4Fe_4S_3(S_2)^{2+}$, although in their case the movement of the Fe−Fe bond is coupled to structural changes in the S_2 ligand.

The second major result comes from DNMR studies of the mixed valence species $\mathbf{1Me}^{3+}$ in the context of our previous studies on $(MeC_5H_4)_4Ru_4S_4^{2+}$. Our experiments on the trication also shed light on the mechanics of the M−M bond movement. For $\mathbf{1Me}^{3+}$, metal−metal bond movement occurs via either a delocalized intermediate or at least two localized pathways.

Previous examples of mobile metal−metal bonds[1,2,7] could always be explained by pathways involving the movement of a single metal−metal bond. This work provides one definite and one likely example where the dynamics require the migration of more than one metal−metal bond.

Experimental Section

Instrumental and procedural details may be found in previous papers.[7] Dynamic ^{1}H NMR measurements on $[\mathbf{1Me}](PF_6)_2OTf$ were collected with 64 000 data points, a 32 μs pulse width, and a 2 s delay time. Variable-temperature ^{1}H NMR measurements on $\mathbf{1Me}^+$ were collected with 32 000 data points, a 6.1 μs pulse width, and a 1 s delay time. Samples for ^{1}H NMR measurements were prepared by dissolving ~18 mg of the cluster salt in ~0.8 mL of deuterated solvent which had been dried over 4A molecular sieves. MeOTf was used as obtained from Aldrich. $(MeC_5H_4)_4Ru_4S_4$ was prepared as described in the literature.[9] All other chemicals used were of reagent grade. Unless otherwise stated all operations were carried out under a N_2 atmosphere. Mass spectral results are reported in units of *m/z*; 3-nitrobenzyl alcohol was the matrix.

Magnetization Transfer NMR Experiments. Magnetization transfer experiments were carried out at five temperatures (18, 30, 40, 50,

(16) A useful reference compound for this family of compounds is the cubane $[Re(SMe)(CO)_3]_4$: Harrison, W.; Marsh, W. C.; Trotter, J. *J. Chem. Soc., Dalton Trans.* **1972**, 1009.
(17) van den Berg, W.; van der Linden, J. G. M.; van Riessen, B. A.; de Bruin, B.; Bosman, W. P.; Smits, J. M. M.; Beurskens, P. T. *Inorg. Chem.* **1993**, *32*, 3637.
(18) Blonk, H. L.; Mesman, J.; van der Linden, J. G. M.; Steggerda, J. J.; Smits, J. M. M.; Beurskens, G.; Beurskens, P. T.; Tonon, C.; Jordanov, J. *Inorg. Chem.* **1992**, *31*, 962. Ogino, H.; Tobita, H.; Yanagisawa, K.; Shimoi, M.; Kabuto, C. *J. Am. Chem. Soc.* **1987**, *109*, 5847. Trinh-Toan; Teo, B. K.; Ferguson, J. A.; Meyer, T. J.; Dahl, L. F. *J. Am. Chem. Soc.* **1977**, *99*, 408.
(19) In this very interesting case the Fe−Fe bonds are adjacent both in the neutral and monocation states: Inomata, S.; Tobita, H.; Ogino, H. *Inorg. Chem.* **1992**, *31*, 722.
(20) Garito, A. F.; Heeger, A. J. *Acc. Chem. Res.* **1974**, *7*, 232.
(21) Koide, Y.; Bautista, M. T.; White, P. S.; Schauer, C. K. *Inorg. Chem.* **1992**, *31*, 3690.
(22) Ohst, H. H.; Kochi, J. K. *J. Am. Chem. Soc.* **1986**, *108*, 2897.
(23) Pullinam, C. R.; Thoden, J. B.; Stacy, A. M.; Spencer, B.; Englert, M. H.; Dahl, L. F. *J. Am. Chem. Soc.* **1991**, *113*, 7398.

and 60 °C). The resonance at 1.6 ppm was irradiated, and the decrease in the intensity of the peak at 2.1 ppm was determined. We assumed that at 18 °C there is no exchange, since no intensity change was observed. The $t_{1/2}$ values were determined for each peak at the various temperatures and are shown below. The rate constants were calculated from the degree of saturation according to the following relation:[24]

$$1/k = \tau = T_{1A}\left(\frac{M_{zA}}{M_{0A} - M_{zA}}\right)$$

where M_{0A} = intensity before irradiation, MZ_A = intensity after irradiation, T_{1A} = spin lattice relaxation time, and k = rate constant describing the exchange process.

M_{0A}	M_{zA}	T (K)	k (s^{-1})
143	110	303	0.08
120	53	313	0.33
95	23	323	0.78
70	7	333	2.14

The term $\ln(kNh/RT)$ varied linearly with T^{-1}. From this plot, the activation parameters $\Delta S^{\ddagger}$ and $\Delta H^{\ddagger}$ were calculated. Error analysis assumed a 10% error in rate constant. The temperature of the NMR probe had been previously calibrated using a methanol standard, and the error in temperature was estimated at 2 K. Errors were computed by Girolami's method.[25]

Electrochemical Methods. Cyclic voltammetry measurements were performed on a Bioanalytical Systems BAS-100 electrochemical analyzer using a Ag/AgCl reference electrode and platinum auxiliary and working electrodes with 0.1 M Bu_4NPF_6 supporting electrolyte. Cyclic voltammograms were recorded with a scan rate of 100 mV/s. Differential-pulse voltammetry employed a Bioanalytical Systems BAS-50W under the following conditions: 50 ms pulse width, current sampled 200 ms after pulse was applied, sweep rate of 5 mV/s, pulse amplitude of 10 mV, sample width of 17 ms, and a quite time of 2 s. The DPV experiment also utilized a Ag/AgCl reference electrode and platinum auxiliary and working electrodes with 0.1 M Bu_4NPF_6.

$[(MeC_5H_4)_4Ru_4S_3(SMe)]OTf$ (1Me$^+$). A solution of 0.250 g (0.294 mmol) of $(MeC_5H_4)_4Ru_4S_4$ in 30 mL of CH_2Cl_2 was treated with 33 μL (0.292 mmol) of MeOTf. Immediately the solution color changed from red to brown. After 30 min the crude product was precipitated with 60 mL of hexanes. The product was recrystallized from 10 mL of acetone by the addition of 30 mL of hexanes. Yield: 0.259 g (87%). Anal. Calcd for $C_{26}H_{31}F_3O_3Ru_4S_5$: C, 30.83; H, 3.08; S, 15.82. Found: C, 30.90; H, 3.16; S, 15.06. UV−vis (CH_3CN, nm): 242, 316, 420. ^{1}H NMR (CD_3CN, 20 °C): δ 1.61 (s, 3H, $CH_3C_5H_4$), 1.97 (s, 3H, $CH_3C_5H_4$), 2.07 (s, 6H, $CH_3C_5H_4$), 2.72 (s, 3H, SCH_3), 3.99 (m, 2H, $CH_3C_5H_4$), 4.32 (m, 2H, $CH_3C_5H_4$), 4.59 (m, 2H, $CH_3C_5H_4$), 4.63 (m, 2H, $CH_3C_5H_4$), 4.77 (m, 2H, $CH_3C_5H_4$), 4.94 (m, 4H, $CH_3C_5H_4$), 5.65 (m, 2H, $CH_3C_5H_4$). $^{13}C\{^1H\}$ NMR (CD_3CN): δ 12.86 (s, 5C, $CH_3C_5H_4$), 12.92 (s, 5C, $CH_3C_5H_4$), 12.93 (s, 10C, $CH_3C_5H_4$), 35.19 (s, SCH_3), 82.02 (s, $CH_3C_5H_4$), 84.01 (s, $CH_3C_5H_4$), 85.08 (s, $CH_3C_5H_4$), 85.53 (s, $CH_3C_5H_4$), 85.90 (s, $CH_3C_5H_4$), 87.76 (s, $CH_3C_5H_4$), 86.81 (s, $CH_3C_5H_4$), 87.21 (s, $CH_3C_5H_4$), 105.10 (s, $CH_3C_5H_4$), 105.30 (s, $CH_3C_5H_4$), 105.66 (s, $CH_3C_5H_4$). FABMS: 867 (M^+), 852 (M^+ − Me), 773 (M^+ − MeC_5H_4, − Me).

$[(MeC_5H_4)_4Ru_4S_3(SMe)](PF_6)_2OTf$ ([1Me]$(PF_6)_2$OTf). A 100 mL Schlenk flask was charged with 0.40 g (0.39 mmol) of $[(MeC_5H_4)_4Ru_4S_3(SMe)]OTf$ and 0.260 g (0.79 mmol) of $(C_5H_5)_2FePF_6$ followed by 10 mL of MeCN, giving a green-brown solution. After 30 min the solvent was removed in vacuo, leaving a dark green residue, which was twice recrystallized by dissolution in 10 mL of acetone followed by addition of 30 mL of hexanes. Yield: 0.38 g (74%). Anal. Calcd for $C_{26}H_{31}F_{15}O_3P_2Ru_4S_5$: C, 23.97; H, 2.40; S, 12.30. Found: C, 24.32; H, 2.49; S, 12.26. UV−vis (CH_3CN, nm): 240, 286. ^{1}H NMR (CD_3NO_2, −25 °C): δ 6.75 (m, 1H, MeC_5H_4), 6.49 (m, 1H, MeC_5H_4), 6.41 (m, 1H, MeC_5H_4), 6.16 (m, 1H, MeC_5H_4), 6.08 (m, 1H, MeC_5H_4), 6.03 (m, 1H, MeC_5H_4), 5.93 (m, 1H, MeC_5H_4), 5.85 (m, 1H, MeC_5H_4), 5.84 (m, 1H, MeC_5H_4), 5.73 (m, 1H, MeC_5H_4), 5.68 (m, 1H, MeC_5H_4), 5.58 (m, 2H, MeC_5H_4), 5.57 (m, 1H, MeC_5H_4), 5.47 (m, 1H, MeC_5H_4), 5.07 (m, 1H, MeC_5H_4), 3.14 (s, 3H, SCH_3), 2.39 (s, 3H, $CH_3C_5H_4$), 2.36 (s, 3H, $CH_3C_5H_4$), 2.29 (s, 3H, $CH_3C_5H_4$), 1.89 (s, 3H, $CH_3C_5H_4$). ^{1}H NMR (CD_3NO_2, 95 °C): δ 6.17 (m, 2H, MeC_5H_4), 6.0 (broad s, 8 H, MeC_5H_4), 5.84 (broad s, 6H, MeC_5H_4), 3.22 (s, 3H, SCH_3), 2.42 (s, 3H, $CH_3C_5H_4$), 2.26 (broad s, 9H, $CH_3C_5H_4$). $^{13}C\{^1H\}$ NMR (CD_3NO_2, −25 °C): δ 123.63 (s, MeC_5H_4), 123.02 (s, MeC_5H_4), 116.85 (s, MeC_5H_4), 116.70 (q, CF_3SO_3−), 116.56 (s, MeC_5H_4), 96.28 (s, MeC_5H_4), 95.65 (s, MeC_5H_4), 95.55 (s, MeC_5H_4), 94.88 (s, MeC_5H_4), 94.10 (s, MeC_5H_4), 93.57 (s, MeC_5H_4), 93.39 (s, MeC_5H_4), 93.09 (s, MeC_5H_4), 92.81 (s, MeC_5H_4), 92.25 (s, MeC_5H_4), 92.10 (s, MeC_5H_4), 91.99 (s, MeC_5H_4), 91.38 (s, MeC_5H_4), 91.02 (s, MeC_5H_4), 89.82 (s, MeC_5H_4), 89.05 (s, MeC_5H_4), 36.65 (s, μ_3-SCH_3), 14.52 (s, $CH_3C_5H_4$), 14.41 (s, $CH_3C_5H_4$), 13.41 (s, $CH_3C_5H_4$), 13.33 (s, $CH_3C_5H_4$). FABMS: 867 (M^+), 852 (M^+ − Me), 773 (M^+ − MeC_5H_4, −Me).

X-ray Crystallography of $[(MeC_5H_4)_4Ru_4S_3(SMe)]OTf$. Single crystals of $[(MeC_5H_4)_4Ru_4S_3(SMe)]OTf$ were obtained by slow diffusion of hexanes into a concentrated acetone solution. Data were collected on an opaque black plate of dimensions 0.03 × 0.2 × 0.4 mm^3 mounted on a glass fiber. [1Me](OTf) crystallizes in the space group $P2_1/a$ with a = 14.767(1), b = 15.383(1), c = 15.755(1) Å; $\alpha = \gamma = 90$, β = 115.859(2)°; Z = 4; and d_{calcd} = 2.089 g/cm^3. Four thousand eight hundred seventy-six unique reflections were refined to a final R = 0.051 and R_w = 0.062. Selected bond distances and angles are listed in Table 1. Selected atomic coordinates are presented in Table 3. The structure was solved by direct methods (SHELXS-86); correct ruthenium positions were deduced from an E-map. Subsequent least-squares refinements and difference Fourier syntheses revealed positions for the remaining non-hydrogen atoms. Disordered MeC_5H_4 ring atom positions were "idealized" and refined as rigid groups; relative site occupancy from group "A" converged at 0.64(1). Disordered anion positions were constrained to "ideal" bond lengths and bond angles and refined as rigid groups; relative site occupancy for group "B" converged at 0.638(7). Hydrogen atoms were included as fixed contributors in idealized positions. In the final cycle of least-squares refinement, anisotropic thermal coefficients were refined for anion atoms by element, for disordered cyclopentadienyl carbon atoms by type, and for methyl and aromatic hydrogen atoms. Successful convergence was indicated by the maximum shift/error for the last least-squares cycle. No extinction correction was applied; however, a numerical absorption correction was applied, with maximum and minimum transmission factors of 0.942 and 0.607, respectively. The highest peaks on the map were in the vicinity of the anion; the final map had no other significant features. A final analysis of variance between observed and calculated structure factors showed a slight dependence on $\sin(\theta)$.

Table 3. Selected Atomic Coordinates for 1Me$^+$

	x/a	y/b	z/c
Ru1	0.11869(6)	0.17776(6)	0.85750(6)
Ru2	0.09614(7)	−0.01480(6)	0.71520(7)
Ru3	−0.02048(6)	−0.02484(6)	0.81430(6)
Ru4	−0.05666(7)	0.17700(6)	0.68856(6)
S1	0.1378(2)	0.0287(2)	0.8649(2)
S2	0.1035(2)	0.1412(2)	0.7066(2)
S3	−0.0404(2)	0.1274(2)	0.8327(2)
S4	−0.0706(2)	0.0254(2)	0.6626(2)
C1	0.2441(9)	−0.0221(10)	0.9623(9)

Acknowledgment. This research was supported by the National Science Foundation. We thank Gregory Girolami for many helpful discussions and Michael Spencer for assistance with the computer analysis of the NMR line shapes.

Supporting Information Available: Tables of extended listings of crystal and data collection details, bond angles and distances, and thermal parameters (9 pages). Ordering information is given on any current masthead page.

IC950332I

(24) Martin, M. L. *Practical NMR Spectroscopy*; Heyden: London, 1980; pp 315−318.
(25) Morse, P. M.; Spencer, M. H.; Wilson, S. R.; Girolami, G. S. *Organometallics* **1994**, *13*, 1646.